



Research

**Cite this article:** Woolley TE. 2025 BespokeTuring patterns with specific nonlinear properties. *Proc. R. Soc. A* **481**: 20250030.<https://doi.org/10.1098/rspa.2025.0030>

Received: 13 January 2025

Accepted: 25 March 2025

**Subject Areas:**

applied mathematics, mathematical modelling

**Keywords:**

Turing patterns, reaction–diffusion, nonlinear analysis, bifurcations, morphogenesis, simulation

**Author for correspondence:**

Thomas E. Woolley

e-mail: [woolleyt1@cardiff.ac.uk](mailto:woolleyt1@cardiff.ac.uk)

# Bespoke Turing patterns with specific nonlinear properties

Thomas E. Woolley

Cardiff School of Mathematics, Cardiff University Senghennydd Road, CF24 4AG Cardiff, UK

TEW, 0000-0001-6225-5365

Turing patterns offer a mechanism for understanding self-organization in biological systems. However, due to their flexibility, it is a mechanism that can often be abused. Here, we construct a minimal Turing system defined by just four parameters controlling the: diffusion rate, steady state, linear dynamics and nonlinear dynamics. Using just these four parameters, we can construct a set of kinetics with a number of desirable properties. Firstly, we can turn any homogeneous steady state into a Turing unstable steady state. Secondly, we can ensure that the Turing instability appears within any chosen parameter region. Thirdly, this formulation provides an unbounded patterning parameter space with guaranteed positive solutions. Finally, using weakly nonlinear analysis, we demonstrate that if we have freedom in any two of the parameters, then we can define any required pattern transition (i.e. spots-to-stripes, or stripes-to-spots) under any given changes of one of the parameters. Thus, if a Turing system is going to be applied to understand a specific biological system and, moreover, if it is going to be used to extrapolate predictions for experimental perturbations, then our findings underscore the necessity of heavily restricting the modelling components and parameter values, since any freedom could be exploited to generate potentially contradictory predictions.

## 1. Introduction

The study of Turing patterns has interested mathematical biologists for decades due to its ability to explain self-organization in diverse biological systems [1,2].

© 2025 The Authors. Published by the Royal Society under the terms of the Creative Commons Attribution License <http://creativecommons.org/licenses/by/4.0/>, which permits unrestricted use, provided the original author and source are credited.

Originally proposed by Turing [3], the theory postulates that diffusion-driven instabilities can transform homogeneous steady states into spatially heterogeneous patterns, providing a mechanism for the emergence of biological structures. Over the years, reaction–diffusion models have been employed to explore phenomena ranging from animal coat markings [4,5] to chemical pre-patterning in developmental biology [6].

Despite the simplicity of Turing’s theory, its broad applicability and flexibility pose challenges for biological interpretation. That is, model selection and parameter identifiability are inherent challenges across all of applied mathematical modelling [7–9], and we will show that with a minimum freedom in parameter definitions we can generate diametrically opposite predictions of how patterns can transition.

While Turing systems can replicate many observed patterns [10–12], the underlying model of partial differential equations (PDEs) and resulting patterning parameter spaces that produce such patterns are often poorly constrained by biological data [13–16]. This freedom allows reaction–diffusion systems to generate a wide range of behaviours, but complicates efforts to identify specific biological pathways, or mechanisms.

Recently, we were able to demonstrate that we could build Turing systems with desired linear properties, so that a pattern could be produced in any desired parameter region [17]. Further, we demonstrated that small variations in boundary conditions and boundary shape were able to completely change the expected Turing instability bifurcation structures and the resulting patterns [18,19]. Thus, Turing systems can be highly sensitive to many factors and, hence greatly adaptable to many biological requirements.

In this work, we build upon these developments by constructing a minimal Turing system with desired linear and nonlinear properties. We demonstrate that the entire system can be defined using four parameters controlling: the diffusion rate; the steady state; the linear dynamics; and the nonlinear dynamics. This minimal parametrization enables us to produce a Turing system with an unbounded patterning parameter space that only produces positive trajectories. Moreover, using weakly nonlinear analysis, we demonstrate that if we have freedom in any two of the parameters we are able to account not only for what pattern we would like to see initially bifurcate (spots or stripes), but also we can specify desired parameter relationships (e.g. increases in one coupled with decreases in another) that will lead to defined pattern transitions of either spots-to-stripes or stripes-to-spots, leading us to question the predictability of models that use these observable biological transitions to justify their systems [10,12].

This work can be compared with that of the BVAM model [20–22], which is a mathematically motivated polynomial set of kinetics that included terms up to cubic order. The BVAM model has had great success in obtaining patterns that match a variety of fish skin patterns [16], including ‘isolated’ spot patterns that are outside the normal spot and stripe Turing patterns that have a fairly consistent wavelength [23]. In contrast to the BVAM work, which investigates what a general cubic system can achieve [24], we restrict the number of available parameters and show much of this complexity can be achieved with fewer degrees of freedom.

## 2. Theory

We are looking to create a generic system of reaction–diffusion equations that will not only present a Turing pattern within a desired parameter region (defined by the linear analysis) but also satisfy certain nonlinear properties, such as pattern selection, at least in the weakly nonlinear regime. In the following, we restrict ourselves to working with two populations,  $u$  and  $v$ , interacting on a Euclidean space,  $\Omega$ , which is either a finite line, or square (depending on dimension). Further, the system will have zero-flux boundary conditions defined on the boundary,  $\partial\Omega$  and initial conditions defined by noise.

These restrictions ensure that we are using as simple a system as possible. That is, a Turing system requires at least two interacting populations [25] but it has been demonstrated that adding more morphogen populations can greatly increase the complexity of the solutions [26–28].

The random initial conditions ensure that we are not feeding the system-specific unstable wave modes and enforcing a pre-pattern, while the boundary conditions ensure that the boundaries play a minimal role. By restricting the system's components and defining as little specificity about the system as possible we will demonstrate the range of complexity that is generically present. These simplifications also allow the analysis to be tractable since dependence of the pattern formation of the domain size and boundary conditions can only be calculated exactly in simple polygonal geometries [19,29]. Although restrictive we will demonstrate that we are able to generate all the required complexity within this situation and, thus, more complicated patterns can easily be generated by providing more specific domain shapes, boundary conditions and initial conditions [18,30,31].

Let  $u(x, t)$  and  $v(x, t)$  be the two interacting morphogen populations that exist for all  $x \in \Omega$  and for all time  $t > 0$ . The evolution of  $u$  and  $v$  is defined by interaction equations  $f$  and  $g$  combined with spatial diffusion at rates  $D_u$  and  $D_v$ , respectively, through

$$\frac{\partial u}{\partial t} = D_u \nabla^2 u + f(u, v) \quad (2.1)$$

and

$$\frac{\partial v}{\partial t} = D_v \nabla^2 v + g(u, v), \quad (2.2)$$

where  $\nabla^2$  is the Laplacian on  $\Omega$ . Depending on the spatial dimension,

$$\nabla^2 = \frac{\partial^2}{\partial x^2} \quad \text{when } \Omega \in \mathbb{R} \quad (2.3)$$

and

$$\nabla^2 = \frac{\partial^2}{\partial x^2} + \frac{\partial^2}{\partial y^2} \quad \text{when } \Omega \in \mathbb{R}^2, \quad (2.4)$$

where  $x$  and  $y$  are the standard Cartesian coordinates.

For simplicity, we assume that  $\Omega$  is insulated leading to zero-flux boundary conditions,

$$\frac{\partial u}{\partial \mathbf{n}} = 0 = \frac{\partial v}{\partial \mathbf{n}} \quad \text{on } \delta\Omega, \quad (2.5)$$

where  $\partial/\partial \mathbf{n}$  is the directional derivative along the outward pointing normal vector,  $\mathbf{n}$ , defined on  $\delta\Omega$  [32]. These boundary conditions mean that the morphogens are reflected by the boundary and do not pass through, or stick to  $\delta\Omega$ . To complete the system's definition, we need to supply an initial condition; however, this first requires us to define a Turing instability.

**Definition 2.1 (Turing instability).** A system of PDEs presents a Turing instability if there is a uniform spatial steady state that is stable in the absence of diffusion, which can be driven unstable by the inclusion of diffusion.

In our case, the spatially uniform steady state is labelled  $(u_s, v_s)$ . The initial condition is then assumed to be a small random perturbation about this point,

$$(u(x, 0), v(x, 0)) = |(u_s, v_s) + (\eta_u(x), \eta_v(x))|, \quad (2.6)$$

where  $\eta_u(x)$  and  $\eta_v(x)$  are samples from a uniform random distribution on the interval  $[-0.1, 0.1]$ . The absolute value is to ensure that the initial condition is never negative.

## (a) Linear analysis

Under the set-up of §2, we can use standard linear analysis [33] to derive the Turing inequalities that must be satisfied to ensure a Turing instability [5]. Specifically, we use an expansion of the form

$$\begin{pmatrix} u \\ v \end{pmatrix} = \begin{pmatrix} u_s \\ v_s \end{pmatrix} + \exp(\lambda t) \cos(\mathbf{k} \cdot \mathbf{x}) \begin{pmatrix} \epsilon_u \\ \epsilon_v \end{pmatrix}, \quad (2.7)$$

in the two cases of (i) without diffusion,  $D_u = D_v = 0$ , and (ii) with diffusion,  $D_u \neq 0 \neq D_v$ . We aim to derive conditions under which the sign of the real part of  $\lambda$  is negative in case (i), indicating that

$(u_s, v_s)$  is stable, and positive in case (ii), indicating that  $(u_s, v_s)$  is unstable to spatial perturbations. Further, since  $\Omega$  is either a line of length  $l$  ( $\Omega = [0, l]$ ) or a square of side length  $l$  ( $\Omega = [0, l] \times [0, l]$ ) then, to satisfy the zero-flux boundary conditions on  $\partial\Omega$ , we require that  $k = k = n\pi/l$ , or  $k = (n\pi/l, m\pi/l)$ , in one and two dimensions, respectively, where  $n, m \in \mathbb{Z}$ .

Following the standard ‘Turing analysis’ [5], we can derive that a Turing instability occurs if

$$f_u + g_v < 0, \quad (2.8)$$

$$f_u g_v - f_v g_u > 0, \quad (2.9)$$

$$D_v f_u + D_u g_v > 0, \quad (2.10)$$

$$(D_v f_u + D_u g_v)^2 - 4D_u D_v (f_u g_v - g_u f_v) > 0 \quad (2.11)$$

and  $\exists n > 0$  such that  $k_-^2 < \left(\frac{n\pi}{l}\right)^2 < k_+^2$

$$\text{where } k_{\pm}^2 = \frac{D_v f_u + D_u g_v \pm \sqrt{(D_v f_u + D_u g_v)^2 - 4D_u D_v (f_u g_v - g_u f_v)}}{2D_u D_v}, \quad (2.12)$$

where the subscripts on the  $f$  and  $g$  functions represent partial derivatives with respect to the subscript and all of the derivatives are evaluated at the homogeneous steady state. Inequalities (2.8) and (2.9) ensure that the homogeneous steady state is stable in the absence of diffusion. Inequalities (2.10) and (2.11) ensure that diffusion can drive the homogeneous steady state unstable. Inequality (2.12) ensures that the space is big enough to allow a pattern to form, which is not too restrictive since as long as  $k_{\pm}$  exist (guaranteed by equations (2.10) and (2.11)) we can always find a domain size large to satisfy inequality (2.11), thus, we focus on satisfying inequalities (2.8)–(2.11).

## (b) Arbitrary steady state and positive trajectory

We now begin restricting  $f$  and  $g$  by defining a number of requirements on the system. Previously [17], we demonstrated that we could produce a Turing bifurcation in any parameter region and we will inherit this requirement. However, we did not demonstrate that a Turing instability could occur at any defined spatially uniform steady state. To impose a spatially uniform steady state, we require that  $(u_s, v_s)$  is a solution to  $f(u_s, v_s) = g(u_s, v_s) = 0$ . There are many ways to achieve this; however, one of the simplest ways is to ensure that  $f$  and  $g$  are polynomials with  $(u_s, v_s)$  as a root,

$$f = (u - u_s)f_1(u, v) + (v - v_s)f_2(u, v) \quad (2.13)$$

and

$$g = (u - u_s)g_1(u, v) + (v - v_s)g_2(u, v). \quad (2.14)$$

In the simplest case, we could make the  $f_i$  and  $g_i$  constants and, so, the Jacobian (matrix of the first-order partial derivatives) of the system at  $(u_s, v_s)$  would be

$$\begin{aligned} J &= \begin{pmatrix} f_u & f_v \\ g_u & g_v \end{pmatrix} \Big|_{(u_s, v_s)}, \\ &= \begin{pmatrix} f_1 & f_2 \\ g_1 & g_2 \end{pmatrix}. \end{aligned} \quad (2.15)$$

Hence, through judicious choice of the  $f_i$  and  $g_i$  we can satisfy inequalities (2.8)–(2.11), which is eminently possible as we would have six parameters,  $(D_u, D_v, f_1, f_2, g_1, g_2)$ , to satisfy four inequalities. However, without nonlinearities restricting the growth of the instability the population would simply grow without bound.

Thus, nonlinearities are essential, but unless they are specified carefully [34], they will cause the nullcline (lines along which  $f$  or  $g$  are zero) to cross more than once, resulting in more than one steady state. However, we can use these extra roots and nullclines to ensure that the populations

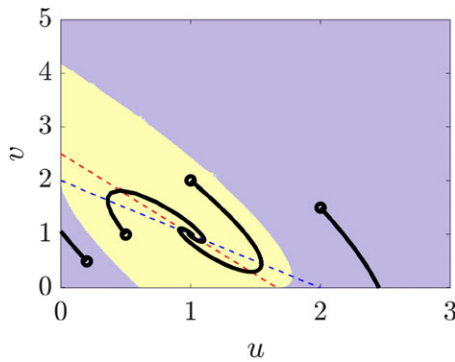


**Figure 1.** Phase plane of an ODE system with kinetics defined by equations (2.16) and (2.17) illustrating four trajectories (black lines) starting from four different initial conditions (black circles). The light-yellow region illustrates the basin of attraction of non-trivial steady state, i.e. all the initial conditions that will lead to a trajectory terminating at (1,1). The light-blue region represents initial conditions that lead to a trajectory which terminates on an axis. Parameters are  $(f_1, f_2, g_1, g_2, u_s, v_s) = (1, 1, -3, -2, 1, 1)$ .

are always positive. Although unspecified here, the morphogen populations usually represent physical quantities, e.g. protein concentrations, or biomass [14,15,35,36], thus we further restrict  $f$  and  $g$  to ensure that no solution trajectory can become negative. This is achieved by making the  $u = 0$  and  $v = 0$  axes nullclines,

$$f = (u - u_s)uvf_1(u, v) + (v - v_s)uvf_2(u, v) \quad (2.16)$$

and

$$g = (u - u_s)uvg_1(u, v) + (v - v_s)uvg_2(u, v). \quad (2.17)$$

Note we do not have to provide each kinetic function with a  $uv$  term, we could have, for example, made  $u = 0$  a nullcline of  $f$  and  $v = 0$  a nullcline of  $g$ . However, in the case where each axis is only the nullcline of one of the populations then although one population's dynamics is fixed on an axis the other population is free to grow without bound. Further, we know that this growth must be possible since corollaries to inequalities (2.8)–(2.11) prove that one of the populations must have a positive feedback influence on itself [37]. Should one of the populations become zero the  $uv$  terms in equations (2.16) and (2.17) will cause equations (2.1) and (2.2) to simplify to diffusion, which ensures that the solutions of the PDEs will remain positive.

With making the axes nullclines, we have introduced two infinite families of steady states, where at least one of the populations is zero, these will be termed trivial steady states. As the amplitude of the pattern grows, these extra steady states may influence the appearance of Turing patterns, since beyond the initial instability, the patterning solution may not be well characterized by the linear analysis of the steady state [38]. However, since Turing patterns bifurcate continuously from a zero amplitude solution then, at least in the weakly nonlinear parameter regime, Turing patterns will occur. Figure 1 illustrates a phase plane example of the dynamics of equations (2.16) and (2.17) assuming that  $f_i$  and  $g_i$  are simply constants that satisfy inequalities (2.8)–(2.11). We observe that the non-trivial steady state has a non-trivial basin of attraction and, thus, will support Turing patterns, as long as the parameters are near their bifurcation values. Moreover, although  $(u_s, v_s)$  is stable, as desired, the stability of the trivial steady states depend on the position of the initial condition relative to  $(u_s, v_s)$ .

Another feature that has been introduced through making the axes nullclines is that system equations (2.16) and (2.17) have no external source, or sink, as there is no independent constant term in the kinetics that does not multiply a  $u$ , or  $v$ . This implies that the system can pattern in complete isolation, unlike current experimental systems that rely on continuously feeding reagents into the reaction site [39–41].

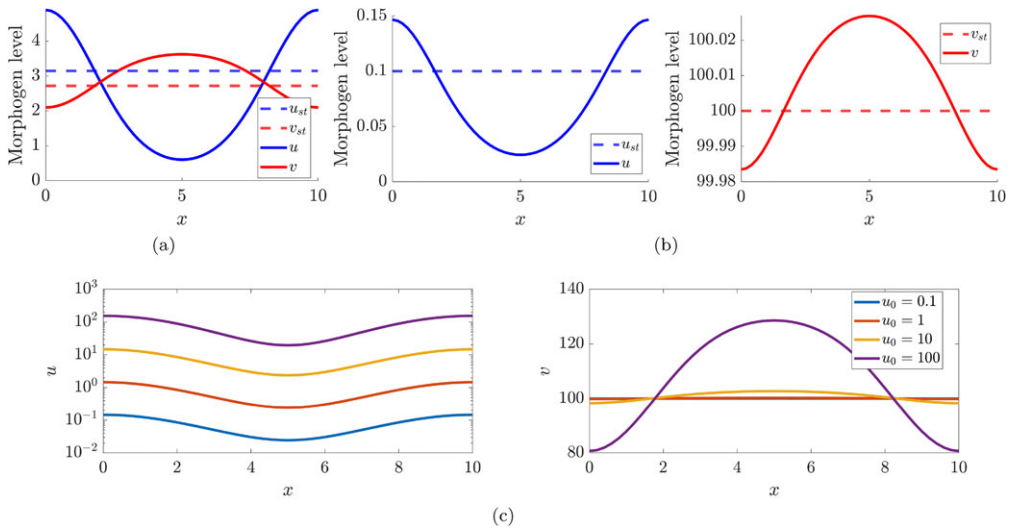


**Figure 2.** Simulations of equations (2.18) and (2.19) with (a)  $(u_s, v_s) = (\pi, e)$ , (b)  $(u_s, v_s) = (0.1, 100)$  and (c)  $u_i = 0.1, 1, 10, 100$  and  $v_s = 100$ , see legend in each subfigure for further details. Other parameters,  $(f_1, f_2, g_1, g_2) = (1, 1, -3, -2)$ , are the same across all cases.

If we now scale the  $f_i$  and  $g_i$  functions such that  $f_i \mapsto f_i/(u_s v_s)$  and  $g_i \mapsto g_i/(u_s v_s)$  the system becomes

$$f = (u - u_s) \frac{u}{u_s} \frac{v}{v_s} f_1(u, v) + (v - v_s) \frac{u}{u_s} \frac{v}{v_s} f_2(u, v) \quad (2.18)$$

and

$$g = (u - u_s) \frac{u}{u_s} \frac{v}{v_s} g_1(u, v) + (v - v_s) \frac{u}{u_s} \frac{v}{v_s} g_2(u, v). \quad (2.19)$$

and, so, the Jacobian is, once again

$$J = \begin{pmatrix} f_u & f_v \\ g_u & g_v \end{pmatrix} \Big|_{(u_s, v_s)} = \begin{pmatrix} f_1 & f_2 \\ g_1 & g_2 \end{pmatrix} \Big|_{(u_s, v_s)}.$$

Thus, as long as we choose the  $f_i(u_s, v_s)$  and  $g_i(u_s, v_s)$  to satisfy inequalities (2.8)–(2.11), any  $(u_s, v_s)$  can undergo a Turing instability using kinetics equations (2.18) and (2.19). At this point, we drop the dependence of  $f_i$  and  $g_i$  on  $(u, v)$  as it is not required to achieve the current goal. Moreover, we assume that none of these kinetic variables are zero.

We demonstrate the ability of equations (2.18) and (2.19) to produce Turing patterns around arbitrary steady states in figure 2. In figure 2a, we choose the patterns to occur around the mathematical constants  $(\pi, e)$ , whereas in figure 2b we demonstrate that the chosen steady states can be chosen arbitrarily separated as  $(u_s, v_s) = (0.1, 100)$ . In each figure, the solid line represents the spatial distribution of morphogen and forms a heterogeneous pattern around its accompanying dashed steady state. Although the patterns were expected, the variation in pattern amplitude may not be. Specifically, the amplitude of the patterns in figure 2a are much greater than those in figure 2b even though the steady state of  $v$  in figure 2b is much larger than that of figure 2a.

Intuitively, the reason for both morphogens in figure 2b to have small amplitude patterns is due to the kinetics having nullclines along  $u = 0$  and  $v = 0$ . Specifically, the  $u$  morphogen has a small steady state (i.e.  $u_s = 0.1$ ) and since the pattern amplitude is bounded below, the difference between the steady state and the minimum must be small. Due to the relative symmetry of the patterns in the weakly nonlinear parameter region, then if the pattern's decrease away from the steady state is restricted then its growth will also be restricted, leading to a small amplitude solution for  $u$ . Moreover, if the range of  $u$  is small then its influence on  $v$  must also be small,

meaning any variation in  $v$  must be small (and vice versa) (unless the kinetics are specifically chosen to cause a jump in the order of influence).

The influence of  $u_s$  as a control parameter of the amplitude can be observed in [figure 2c](#), where we have simulated the system with increasing values of  $u_0$ . Note that the  $u$  population plot is on a logarithmic axis, thus, not only is  $u_s$  increasing but the amplitude of the pattern is as well. Comparing the  $u$  and  $v$  population plots of [figure 2c](#), we see that although the  $v$  population's steady state is not altered its amplitude increases as  $u_s$  does. In fact the amplitude of the  $v$  population is so small in the cases of  $u_s = 0.1$  and  $1$  that the lines practically lie on top of  $v_s = 100$  ([figure 2b](#)).

Having shown that we can produce Turing patterns around any steady state, we can simply map  $(u_s, v_s)$  to  $(1,1)$  through scaling  $u = u_s U$  and  $v = v_s V$ . Further, to ensure that the Jacobian remains as in [equation \(2.15\)](#) we must also rescale the  $f_i$  and  $g_i$ ,

$$f_1 \mapsto \frac{f_1}{u_s}, f_2 \mapsto \frac{f_2}{v_s}, g_1 \mapsto \frac{g_1}{u_s}, g_2 \mapsto \frac{g_2}{v_s},$$

to produce

$$f = (U - 1)UVf_1 + (V - 1)UVf_2 \quad (2.20)$$

and

$$g = (U - 1)UVg_1 + (V - 1)UVg_2. \quad (2.21)$$

Although [equations \(2.20\)](#) and [\(2.21\)](#) are a useful form as it explicitly allows us to control the linear bifurcation without worrying about the steady states, by choosing the non-dimensionalization of [equations \(2.18\)](#) and [\(2.19\)](#) in a different way we can reduce the number of free parameters in the ordinary differential equation (ODE) system from six,  $(D_u, D_v, f_1, f_2, g_1, g_2)$ , to three.

To make progress, we must assume a sign structure for the Jacobian. Up to symmetries and renaming of the variables, [inequalities \(2.8\)](#) and [\(2.11\)](#) require that the Jacobian has one of two specific sign structures [42],

$$\text{sign}(J) = \begin{pmatrix} + & + \\ - & - \end{pmatrix} \text{ or } \begin{pmatrix} + & - \\ + & - \end{pmatrix}.$$

The two sign structures determine whether the peaks and troughs of  $u$  and  $v$  are out of phase, or in phase, respectively [5]. In the following, we assume that our kinetics have the former sign structure, so  $f_i > 0$  and  $g_i < 0$ . The results that follow are equally true for the second sign structure, although appropriate minus signs will have to be tracked.

Letting  $u = (v_s f_2 / f_1)U$ ,  $v = v_s V$ ,  $t = T / f_1$  and introducing  $\alpha = v_s f_2 / (u_s f_1)$ ,  $G_1 = f_2 |g_1| / f_1^2$ ,  $G_2 = |g_2| f_2 v_s / (u_s f_1^2)$  [equations \(2.18\)](#) and [\(2.19\)](#) can be rewritten in the form

$$\frac{dU}{dT} = (U\alpha - 1)UV + \alpha(V - 1)UV \quad (2.22)$$

and

$$\frac{dV}{dT} = -(U\alpha - 1)UVG_1 - \alpha(V - 1)UVG_2. \quad (2.23)$$

Although not as visually 'clean' as [equations \(2.20\)](#) and [\(2.21\)](#), this form has the added advantage that the Jacobian simplifies to

$$J = \begin{pmatrix} 1 & 1 \\ -G_1 & -G_2 \end{pmatrix}. \quad (2.24)$$

Further, non-dimensionalizing the spatial coordinate through  $x = L\sqrt{D_u/f_1}X$  and letting  $D = D_u/D_v$  we produce the system

$$\frac{\partial U}{\partial T} = \frac{1}{L^2} \nabla_X^2 U + (U\alpha - 1)UV + \alpha(V - 1)UV \quad (2.25)$$

and

$$\frac{\partial V}{\partial T} = \frac{D}{L^2} \nabla_X^2 V - (U\alpha - 1)UVG_1 - \alpha(V - 1)UVG_2. \quad (2.26)$$

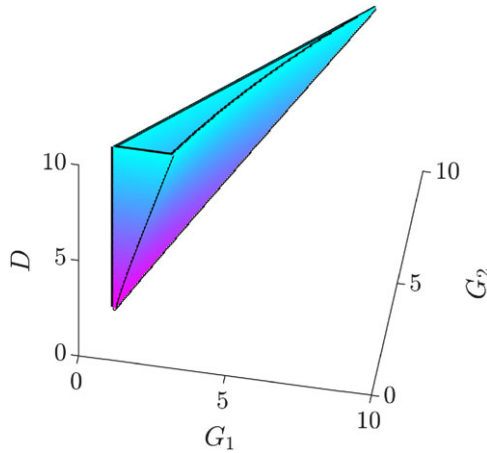


**Figure 3.** Illustrating the Turing patterning parameter region fulfilling [inequalities \(2.27\)](#) and [\(2.28\)](#).

with zero-flux boundary conditions on the line  $[0,1]$ , or square  $[0,1] \times [0,1]$  through the identification that  $L = l/\sqrt{D_u/f_1}$ . Since we will be considering the spatial scale,  $L$  (or equivalently  $l$ ), as the bifurcation parameter, it is also easier to work with the spatially non-dimensionalized system since the non-dimensionalization process establishes the bifurcation parameter as a multiplier of the Laplacian, explicitly, the factors of  $1/L^2$  in [equations \(2.25\)](#) and [\(2.26\)](#).

Thus, any solution of [equations \(2.1\)](#) and [\(2.2\)](#) with kinetics ([equations \(2.16\)](#) and [\(2.17\)](#)) (which allow any point to be made Turing unstable) can be cast into the form of [equations \(2.25\)](#) and [\(2.26\)](#), where the Turing inequalities are simplified to

$$G_1 > G_2 > 1 \quad (2.27)$$

and

$$D > \left( \sqrt{G_1 - G_2} + \sqrt{G_1} \right)^2. \quad (2.28)$$

A corollary to [inequalities \(2.27\)](#) and [\(2.28\)](#) is  $D > G_1 > G_2 > 1$ .

The three-dimensional parameter region satisfying [inequalities \(2.27\)](#) and [\(2.28\)](#) is illustrated in [figure 3](#). We observe that, although for any fixed  $D$  the  $(G_1, G_2)$  parameter region is finite, the patterning parameter space is not bounded in the direction of increasing  $D$ . From a mathematical point of view, this unbounded property has allowed consideration of the limits of  $D_v \rightarrow 0$  [[43,44](#)], providing analytical progress on the existence and stability of asymmetric patterns, the amplitude of which varies across the domain.

From a biological perspective, although we can say that the diffusion rates,  $D_u$  and  $D_v$ , cannot be equal and, moreover,  $D_u > D_v$ , we must appeal to a specific application to provide an upper bound on  $D$  and, thus, restrict the  $(G_1, G_2)$  space. Thus, although we remove the criticism of Turing system's having highly restrictive parameter regions that may be too small to be biologically pertinent [[45](#)] we emphasize that biological knowledge is extremely important in bounding the mathematical possibilities.

Further, it may be expected that in many biological applications  $D \approx 1$  because the modelled morphogens usually have similar properties, meaning that we would expect their diffusion rates to be similar. Although patterns can be made for  $D \gtrsim 1$ , fine-tuning would be required to choose  $G_1$  and  $G_2$  appropriately. More generally, it has been shown that if more active species are added then buffering agents can act to slow down one of the morphogens, resulting in larger values of  $D$  [[28,46](#)]. Once again such abilities highlight the importance of knowing all the biological components at play, since any unmodelled, or unknown agent is able to generalize the patterning conditions.

As mentioned previously, we also need the domain to be ‘big enough’. Using [inequality \(2.12\)](#), the minimum domain size which can support a patterning bifurcation can be shown to be

$$L_c = \frac{\pi\sqrt{2D}}{\sqrt{D - G_2 + \sqrt{(D - G_2)^2 - 4D(G_1 - G_2)}}} = \frac{\pi\sqrt{D - G_2 - \sqrt{(D - G_2)^2 - 4D(G_1 - G_2)}}}{\sqrt{2(G_1 - G_2)}}, \quad (2.29)$$

where the two provided forms of  $L_c$  are equivalent, but useful in different contexts. Further, we note that  $L_c$  does not depend on the steady-state controlling parameter,  $\alpha$ . Equally, the patterning [inequalities \(2.27\)](#) and [\(2.28\)](#) do not depend on  $\alpha$ , thus, we have extended our previous result, that we can use level set curves to parametrize  $G_1$  and  $G_2$  appropriately and satisfy the Turing conditions in any desired parameter region with any desired steady state [17]. Moreover, the features of parameter space and steady state can be independently tuned.

### 3. Weakly nonlinear analysis

Here, we will derive and use weakly nonlinear analysis in one spatial dimension. As all one-dimensional patterns are made of peaks and troughs we only have to consider a scalar wave mode,  $k$ , defining the possible unstable wavelengths (see [inequality \(2.12\)](#)). In §4, we extend the theory to consider two spatial dimensions. Although the algebra is more involved in two dimensions, much of the theory is the same [19,47]. However, we have to take into account that patterns can destabilize in multiple directions leading to the extension of the wave mode to be a vector,  $\mathbf{k}$ .

Assuming that patterned solutions bifurcate continuously at  $L = L_c$  from the homogeneous steady state,  $(U_s, V_s) = (1/\alpha, 1)$ , we can conduct a weakly nonlinear stability analysis on [equations \(2.25\)](#) and [\(2.26\)](#) around the uniform steady state that is valid for domain lengths close to  $L_c$  [18,48–50]. Further, we assume that near  $L_c$  the full system’s solution,  $\mathbf{U} = (U, V)$ , evolves as a slowly varying function of time [51]. These assumptions allow us to expand time, space and the solution in terms of a small parameter,  $0 < \epsilon \ll 1$ ,

$$L = L_c + \epsilon L_1 + \epsilon^2 L_2 + \dots, \quad (3.1)$$

$$\frac{\partial}{\partial T} = \epsilon \frac{\partial}{\partial T_1} + \epsilon^2 \frac{\partial}{\partial T_2} + \dots \quad (3.2)$$

and 
$$\mathbf{U}(x, T_1, T_2) = \begin{pmatrix} U_s \\ V_s \end{pmatrix} + \epsilon \mathbf{U}_1(x, T_1, T_2) + \epsilon^2 \mathbf{U}_2(x, T_1, T_2) + \dots, \quad (3.3)$$

where

$$\mathbf{u}_i = \begin{pmatrix} U_i \\ V_i \end{pmatrix}.$$

As  $\epsilon \rightarrow 0$  convergence of expansions of [equations \(3.1\)–\(3.3\)](#) is assured because we are using simple domain geometries, boundary conditions and smooth kinetics. However, we cannot specify the maximum range of  $\epsilon$  over which the approximation remains valid [51,52].

Using  $f(U, V)$  and  $g(U, V)$  to stand for the kinetics in [equations \(2.25\)](#) and [\(2.26\)](#), we can substitute [equations \(3.1\)–\(3.3\)](#) into system [equations \(2.25\)](#) and [\(2.26\)](#) and collect the different orders of  $\epsilon$ . Here, we only consider the expansions up to third order in  $\epsilon$ ,

$$\mathcal{O}(\epsilon) \quad \mathcal{L}\mathbf{u}_1 = 0, \quad (3.4)$$

$$\begin{aligned} \mathcal{O}(\epsilon^2) \quad \mathcal{L}\mathbf{u}_2 = & \frac{\partial \mathbf{u}_1}{\partial T_1} + \frac{2L_1}{L_c^3} D \frac{\partial^2 \mathbf{u}_1}{\partial X^2} - \frac{U_1^2}{2} \begin{pmatrix} f_{UU} \\ g_{VV} \end{pmatrix} \\ & - U_1 V_1 \begin{pmatrix} f_{UV} \\ g_{UV} \end{pmatrix} - \frac{V_1^2}{2} \begin{pmatrix} f_{VV} \\ g_{VV} \end{pmatrix} \end{aligned} \quad (3.5)$$

$$\begin{aligned} \text{and } \mathcal{O}(\epsilon^3) \quad \mathcal{L}\mathbf{U}_3 = & \frac{\partial \mathbf{U}_1}{\partial T_2} + \frac{\partial \mathbf{U}_2}{\partial T_1} - \left( \frac{3L_1^2 - 2L_2L_c}{L_c^4} \right) \mathbf{D} \frac{\partial^2 \mathbf{U}_1}{\partial X^2} + \frac{2L_1}{L_c^3} \mathbf{D} \frac{\partial^2 \mathbf{U}_2}{\partial X^2} \\ & - \begin{pmatrix} f_{uu}U_1 + f_{uv}V_1 & f_{uv}U_1 + f_{vv}V_1 \\ g_{uu}U_1 + g_{uv}V_1 & g_{uv}U_1 + g_{vv}V_1 \end{pmatrix} \mathbf{U}_2 - \frac{1}{6} \begin{pmatrix} f_{uuu}U_1^3 + f_{vvv}V_1^3 \\ g_{uuu}U_1^3 + g_{vvv}V_1^3 \end{pmatrix} \\ & - \frac{U_1V_1}{2} \begin{pmatrix} f_{uuv} & f_{uvv} \\ g_{uuv} & g_{uvv} \end{pmatrix} \mathbf{U}_1, \end{aligned} \quad (3.6)$$

where

$$\mathbf{D} = \begin{pmatrix} 1 & 0 \\ 0 & D \end{pmatrix}$$

and  $\mathcal{L}$  is a linear operator of the form

$$\mathcal{L} = \frac{1}{L_c^2} \mathbf{D} \frac{\partial^2}{\partial X^2} + \mathbf{J}, \quad (3.7)$$

where  $\mathbf{J}$  is the Jacobian, as defined in equation (2.15). In principle, the approximation cascade could be extended to any level, although approximation accuracy is not guaranteed to increase [53].

Equation (3.4) is essentially a compact form of the linear analysis and shows that  $\mathcal{L}$  has a non-trivial kernel spanned by scalar multiples of

$$\mathbf{U}_1 = a(t_1, t_2) \begin{pmatrix} \Lambda \\ 1 \end{pmatrix} \cos(\pi x), \quad (3.8)$$

where  $\Lambda = L_c^2/(\pi^2 - L_c^2)$  and the amplitude function,  $a$ , is to be determined by a higher-order solvability criterion and we know that  $k = \pi$  because we are considering the first bifurcation. Since  $\mathcal{L}$  has a non-trivial kernel then so will  $\mathcal{L}^T$ . Explicitly,

$$\mathcal{L}^T = \frac{1}{L_c^2} \mathbf{D} \frac{\partial^2}{\partial x^2} + \begin{pmatrix} f_u & g_u \\ f_v & g_v \end{pmatrix}, \quad (3.9)$$

and the kernel of  $\mathcal{L}^T$  is spanned by

$$\boldsymbol{\eta} = \begin{pmatrix} \eta \\ 1 \end{pmatrix} \cos(\pi x), \quad (3.10)$$

where  $\eta = G_1 L_c^2 / (\pi^2 - L_c^2)$ . These basis elements are required to ensure that the equations satisfy a consistency relation [54], that is, for  $\mathcal{L}\mathbf{y} = \mathbf{z}$  to have a solution,  $\mathbf{z}$  must be orthogonal to the basis of  $\text{Ker}(\mathcal{L}^T)$ . Enforcing this orthogonality then provides the solvability criterion. The algebraic manipulations, although simple, are arduous. We provide Maple workbooks [55] and MATLAB code [56] at [https://github.com/ThomasEWoolley/Nonlinear\\_properties](https://github.com/ThomasEWoolley/Nonlinear_properties) for reference.

By defining  $L_1 = 0$  and  $\mathbf{U}_1$  to be a function of  $T_2$  only (independent of  $T_1$ ) then the right-hand side of equation (3.5) is naturally orthogonal to equation (3.10), because the nonlinear terms on the right-hand side of equation (3.5) would all be functions of  $\cos^2(\pi x)$  [57,58], which is orthogonal to  $\cos(\pi x)$  under the inner product defined by

$$\langle \mathbf{a}(x), \mathbf{b}(x) \rangle = \int_0^1 \mathbf{a}(x) \cdot \mathbf{b}(x) \, dx. \quad (3.11)$$

Note that setting  $L_1 = 0$  and  $\mathbf{U}_1(T_2)$  is a sufficient approach to this problem, rather than necessary. Equation (3.5) will, thus, have a family of solutions of the form

$$\mathbf{U}_2 = \begin{pmatrix} c_{u0} \\ c_{v0} \end{pmatrix} + \begin{pmatrix} c_{u2} \\ c_{v2} \end{pmatrix} \cos(2\pi x) + \alpha_1 \mathbf{U}_1, \quad (3.12)$$

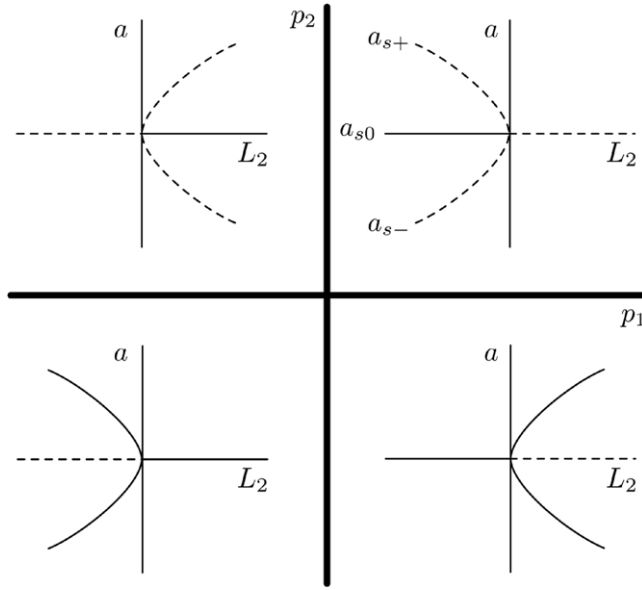


**Figure 4.** Illustrating the stability and existence of the steady states of equation (3.13). The central axis splits the parameter space according to the signs of  $(p_1, p_2)$ , which then alter the bifurcation behaviour of equation (3.13). The dashed curves are the unstable amplitudes and the solid curves are the stable amplitudes.

where  $\alpha_1$  is arbitrary (since  $\mathbf{U}_1$  is in the kernel of  $\mathcal{L}$ ) and set to zero for convenience. Before considering equation (3.6) we must derive the four unknowns,  $c_{u0}$ ,  $c_{v0}$ ,  $c_{u2}$  and  $c_{v2}$  through substitution of equations (3.8) and (3.12) into equation (3.5).

Substituting the derived values of  $\mathbf{U}_s$ ,  $\mathbf{U}_1$  and  $\mathbf{U}_2$  into equation (3.6) and demanding that  $(\eta, \mathcal{L}\mathbf{U}_3) = 0$  we produce the solvability equation for  $a(T_2)$ ,

$$\frac{da}{dT_2} = p_1 L_2 a + p_2 a^3, \quad (3.13)$$

which is the canonical form of a pitchfork bifurcation. We can use linear analysis directly on equation (3.13) to gain more information about the possible amplitudes. The steady states are

$$a_{s0} = 0 \quad \text{and} \quad a_{s\pm} = \pm \sqrt{\frac{-p_1 L_2}{p_2}},$$

illustrating that the existence and stability of the steady states depend on the signs of  $p_1$  and  $p_2$ . The four bifurcation possibilities are illustrated in figure 4.

By definition of the Turing instability the homogeneous steady state is stable for  $L < L_c$ , so, we must be in the case that  $p_1 > 0$ . Although true, it is not obvious from the explicit form of  $p_1$ . In appendix A(a), we demonstrate algebraically that  $p_1 > 0$  is guaranteed within the Turing regime defined by inequalities (2.27) and (2.28).

Since  $p_1 > 0$  the only way the bifurcation structure can change is if  $p_2$  changes sign. However, in appendix A(b), we show that under the kinetics of equations (2.25) and (2.26)  $p_2$  is always negative and, thus, for the Turing bifurcation to become a subcritical bifurcation additional nonlinearities are required.

The supercritical pitchfork bifurcation of equations (2.25) and (2.26) is shown in figure 5 alongside the approximate amplitudes derived from the weakly nonlinear analysis behind equation (3.13). As expected, non-trivial patterns only exist for  $L > L_c$  and the closer  $L$  and  $L_c$  are the better, the better the weakly nonlinear approximation becomes.

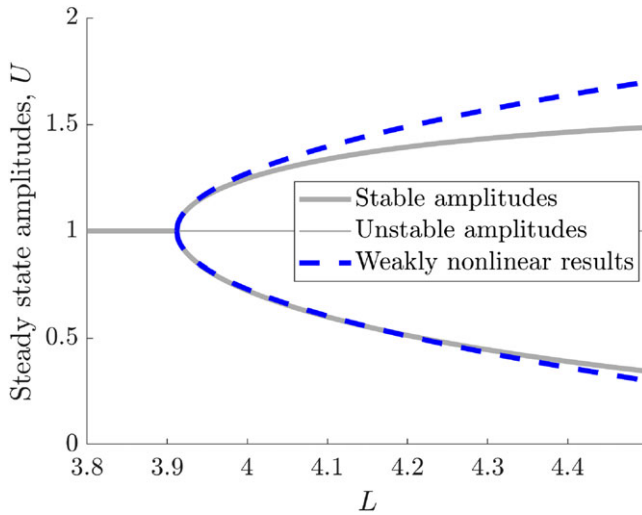


**Figure 5.** Illustrating the pitchfork bifurcation underlying the Turing patterning instability. The grey lines are steady-state amplitudes of equations (2.25) and (2.26), extracted using `pde2path` [59–62], the thick and thin lines are stable and unstable solutions, respectively. The blue dashed line represents the stable state amplitudes of equation (3.13) for  $L > l_c$ . Parameters are  $(\alpha, D, G_1, G_2) = (1, 10, 3, 2)$ .

### (a) Tuning the form of the Turing bifurcation

In §3, we demonstrated that equations (2.25) and (2.26) could only produce supercritical Turing bifurcations. To enable the system to produce subcritical bifurcations, we extend the system to include a higher nonlinearity. We do this to ensure that the introduction of extra term does not influence the steady states, nor the linear analysis.

By including a new parameter, we increase the complexity of the system. To reduce the number of parameters, we consider a single plane within the Turing patterning parameter region of figure 3. Specifically, if we fix

$$G_1 = \frac{D}{4} + \frac{G_2}{2}, \quad (3.14)$$

we remove a degree of freedom and, further, inequality (2.28) is guaranteed to be satisfied, leaving

$$1 < G_2 < \frac{D}{2} \quad (3.15)$$

as the only requirements that need to be satisfied to generate a Turing instability (figure 6). Note, the parameters are non-dimensional, thus, we do not need to worry about incompatible units. Moreover, although we have now reduced the dimensionality of the Turing patterning parameter space, it maintains the critical feature that it is unbounded in  $D$  (figure 6).

Although seemingly ad hoc, equation (3.14) does have reasoning behind it beyond providing a simpler Turing space. Within the fully explicit amplitude equation, one of the re occurring factors (see equation (2.29)) that cannot be simplified is

$$\sqrt{(D - G_2)^2 - 4D(G_1 - G_2)} = \sqrt{D^2 + 2(G_2 - 2G_1)D + G_2^2}.$$

By using equation (3.14), the square-root term simplifies to  $\sqrt{G_2^2} = G_2$  since  $G_2 > 0$ , which, in turn, reduces the number of individual terms in the explicit form of equation (3.13) from over a hundred to

$$\frac{da}{dT_2} = \frac{L_2 \sqrt{2} G_2 a}{\pi(D + 2G_2 - 1)} - \frac{(20\alpha^2 - 11\alpha + 5)G_2 a^3}{6(D + 2G_2 - 1)}. \quad (3.16)$$

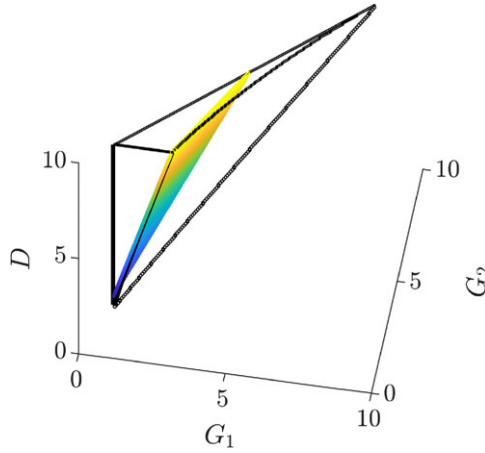


**Figure 6.** Illustrating the two-dimensional Turing patterning parameter region fulfilling inequality (3.15) within the original three-dimensional patterning parameter space defined by inequalities (2.27) and (2.28).

Hence, we continue our investigation using a system of the form

$$\frac{\partial U}{\partial T} = \nabla_X^2 U + (U\alpha - 1)UV + \alpha(V - 1)UV \quad (3.17)$$

and

$$\frac{\partial V}{\partial T} = D\nabla_X^2 V - (U\alpha - 1)UV \frac{(D + 2G_2)}{4} - \alpha(V - 1)UVG_2 + \alpha(V - 1)^2 UVG_3, \quad (3.18)$$

where we note that  $G_3$  can have any real value, positive, negative or zero. The amplitude equation that can be derived from equations (3.17) and (3.18) is

$$\begin{aligned} \frac{da}{dT_2} &= \frac{G_2\sqrt{2}}{\pi(D + 2G_2 - 1)} L_2 a \\ &+ \left( \frac{(28G_2 + 34D)G_3^2}{3(3D + 2G_2)(D - 2G_2)(D + 2G_2 - 1)} - \frac{G_2(20\alpha^2 - 11\alpha + 5)}{6(D + 2G_2 - 1)} \right. \\ &\left. + \frac{((-18\alpha + 9)D^2 + (62\alpha - 46)G_2D + (44\alpha - 40)G_2^2)G_3}{6(3D + 2G_2)(D - 2G_2)(D + 2G_2 - 1)} \right) a^3, \end{aligned} \quad (3.19)$$

which matches equation (3.16) when  $G_3 = 0$ .

As before, we define the coefficients of  $L_2 a$  and  $a^3$  to be  $p_1$  and  $p_2$ , respectively. From §3, we know that the coefficient of  $p_1$  is positive since it is independent of  $G_3$ . Further, since  $p_2$  is a positive quadratic in  $G_3$  then for some  $G_3$  'large enough' (positive or negative) this coefficient must be positive; however, we also know that when  $G_3 = 0$  then  $p_2$  is negative. Hence, for any  $(\alpha, G_2, D)$  there must be values of  $G_3$ , which allow  $p_2$  to take either sign. Specifically, for  $G_3 \in (G_{3-}, G_{3+})$  where

$$\begin{aligned} G_{3\pm} &= \frac{9(2\alpha - 1)D^2 + 2(-31\alpha + 23)G_2D + 2(-22\alpha + 20)G_2^2}{112G_2 + 136D} \\ &\pm \frac{1}{112G_2 + 136D} \left[ 324 \left( \alpha - \frac{1}{2} \right)^2 D^4 + (14088\alpha^2 - 6204\alpha + 3252)G_2D^3 \right. \\ &- 6060G_2^2 \left( \alpha^2 - \frac{92}{505}\alpha + \frac{57}{505} \right) D^2 - 34224G_2^3 \left( \alpha^2 - \frac{267}{713}\alpha + \frac{130}{713} \right) D \\ &\left. - 15984G_2^4 \left( \alpha^2 - \frac{44}{111}\alpha + \frac{20}{111} \right) \right]^{1/2}, \end{aligned} \quad (3.20)$$

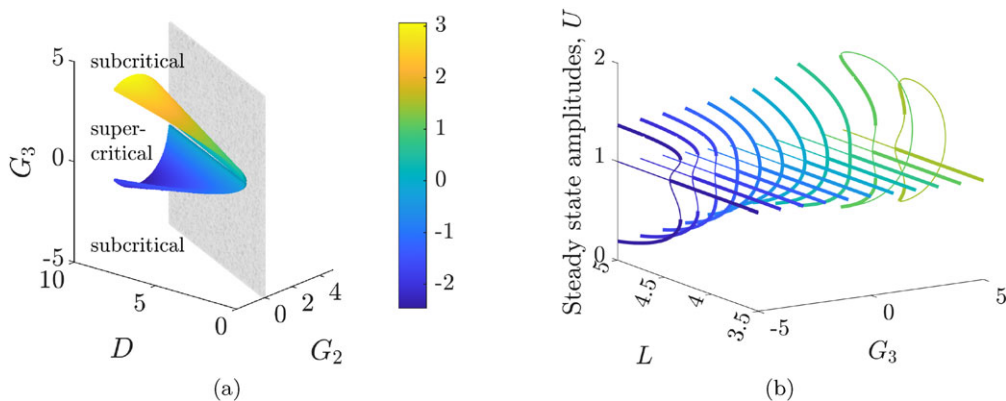


**Figure 7.** Illustrating the subcritical and supercritical pitchfork bifurcations possible as  $G_3$  varies. (a) parameter regions for equations (3.17) and (3.18), when  $\alpha = 1$ . The Turing patterning parameter region is sandwiched between the planes  $G_2 > 1$  (not shown) and  $2G_2 < D$  (grey plane). The two coloured curved planes represent  $G_{3\pm}$  from equation (3.20). The colour of the  $G_{3\pm}$  surfaces represent their values as given on the colour axis. (b) Bifurcation structure of equations (3.17) and (3.18), when  $\alpha = 1, D = 10, G_2 = 2$  with  $G_3 = -5, -4, \dots, 4, 5$ . The thick and thin lines represent the stable and unstable amplitudes, respectively. The colours are to aid discrimination between the curves.

the bifurcation will be a supercritical pitchfork bifurcation ( $p_1 > 0$  and  $p_2 < 0$  in figure 4), and a subcritical pitchfork ( $p_1 > 0$  and  $p_2 > 0$  in figure 4) otherwise. See figure 7a, which illustrates the delineation of the patterning space by  $G_{3\pm}$ .

We observe that the  $G_{3\pm}$  surfaces produce a cone that becomes wider as  $D$  increases, whereby parameters chosen inside the cone lead to supercritical pitchfork bifurcations, while parameters outside the cone lead to subcritical pitchfork bifurcations. This is confirmed by figure 7b where we have extracted the bifurcation structure of equations (3.17) and (3.18) for  $G_3 = -5, -4, \dots, 4, 5$  and we observe that the bifurcations do indeed have a subcritical bifurcation when  $G_3 \leq 3$ , or  $G_3 \geq 4$ . It should also be noted that as  $G_3$  increases the Turing patterns themselves disappear. This can be seen as the curve of steady-state amplitudes forms a closed loop before  $L_c$ . This occurs because as the amplitudes grow the higher-order term,  $(V - 1)^2$  in equation (3.18), being positive, pushes the spatial solution away from the Turing unstable homogeneous state towards the trivial state of  $(\bar{U}, 0)$ , or  $(0, \bar{V})$ , where the values  $\bar{U}$  and  $\bar{V}$  depend on the initial conditions akin to figure 1. However, no such instability appears when  $G_3 < 0$  because the nonlinearity will lead to population reduction if it moves too far from the homogeneous steady state.

## 4. Two dimensions

Large two-dimensional domains offer many potential patterning modes [47,58] providing the Turing pattern's signature sensitivity to initial conditions [2]. However, since we are considering the first patterning bifurcation on a square we are able to restrict the number of patterning modes and their superpositions. As such, due to the symmetry of the square, the nonlinear substitution ansatz will be of the form

$$\mathbf{u} = \mathbf{u}_s + \epsilon(a(T_2) \cos(n\pi x) + b(T_2) \cos(m\pi y)), \quad (4.1)$$

where  $n$  and  $m$  would normally be general integers, so as to satisfy the boundary conditions, but in our case  $n$  and  $m$  are restricted to either 0 or 1. Discounting symmetries there are four possible outcomes:

1.  $n = 0 = m$ , in which case the steady-state perturbation becomes homogeneous and we have already considered the stability of the homogeneous steady state with respect to homogeneous perturbations in §2;
2. either  $n = 0$  or  $m = 0$ , but not both. In this case, the perturbation becomes spatially homogeneous in one direction. Thus, we are considering the ability of the system to generate stripe patterns and the analysis effectively breaks down to the one-dimensional case.
3.  $n = 1 = m$ , in which case we are considering the superposition of two perpendicular stripe solutions, which produce a spot solution.

Proceeding with standard two-dimensional weakly nonlinear analysis with [ansatz \(4.1\)](#) [19,63] we find that the amplitudes are governed by the coupled ODEs

$$\frac{da}{dT_2} = p_1 L_2 a + p_2 a^3 + p_3 b^2 a \quad (4.2)$$

and

$$\frac{db}{dT_2} = p_1 L_2 b + p_2 b^3 + p_3 a^2 b, \quad (4.3)$$

where  $p_1$  and  $p_2$  are as in §3a and

$$\begin{aligned} p_3 = & \frac{4G_3^2}{(D + 2G_2 - 1)(D - 2G_2)} \\ & + \left( \frac{(6D^2 + 6DG_2 - 28G_2^2)\alpha - 3D^2 - 2DG_2 + 8G_2^2}{(D + 2G_2 - 1)(D^2 - 4G_2^2)} \right) G_3 \\ & + G_2 \frac{4\alpha^2 - 7\alpha + 1}{D + 2G_2 - 1}. \end{aligned} \quad (4.4)$$

We note that through setting  $G_3 = 0$  and  $G_2 = 1$  we can quickly demonstrate that  $p_3$  can take either sign by appropriately choosing  $\alpha$ .

We can now approach [equations \(4.2\) and \(4.3\)](#) through standard linear stability methods to understand the possible amplitude bifurcation structures. We find that there are three distinct families of steady states and accompanying eigenvalues,  $\lambda$ , that determine their stability:

1.  $(0, 0)$ , which is the spatially uniform steady states and  $\lambda_0 = p_1 L_2$ . As in §2 and as required by the Turing instability  $(0,0)$  is stable for  $L < L_c$  ( $L_2 < 0$ ) and unstable for  $L > L_c$  ( $L_2 > 0$ );
2.  $(a_1, 0)$ , where  $a_1 = \sqrt{-p_1 L_2 / p_2}$  is the amplitude of the stripe pattern and  $\lambda_{11} = -2p_1 L_2$ ,  $\lambda_{12} = p_1 L_2 (p_2 - p_3) / p_2$ . These match the results derived in §3;
3.  $(a_\bullet, a_\bullet)$ , where  $a_\bullet = \sqrt{-p_1 L_2 / (p_2 + p_3)}$  is the amplitude of the spot pattern and  $\lambda_{\bullet 1} = -2p_1 L_2$ ,  $\lambda_{\bullet 2} = p_1 L_2 (p_3 - p_2) / (p_3 + p_2)$ ,

where we have removed sign symmetries (if  $a_s$  is a steady state then so is  $-a_s$ ) and variable symmetry (if  $a_s$  is a steady state then so is  $b_s = \pm a_s$ ).

Since  $p_1 > 0$  changes in bifurcation structure  $a_1$  and  $a_\bullet$  only depend on the signs of  $p_2, p_3, p_2 + p_3$  and  $p_2 - p_3$ , specifically:

- $a_1$  has a supercritical bifurcation whenever  $p_2 < 0$  and a subcritical bifurcation when  $p_2 > 0$ ;
- $a_\bullet$  has a supercritical bifurcation whenever  $p_2 + p_3 < 0$  and a subcritical bifurcation when  $p_2 + p_3 > 0$ .

Since  $\lambda_{11} = \lambda_{\bullet 1} = -2p_1 L_2$  then in both cases  $L_2 > 0$  is required for the states to be stable. This means that only supercritical bifurcations can be stable. For  $a_1$  to exist we require that  $p_2 < 0$ , while stability requires  $\lambda_{12} < 0$  meaning  $p_2 - p_3 > 0$ . For  $a_\bullet$  to exist we need  $p_2 + p_3 < 0$ , while

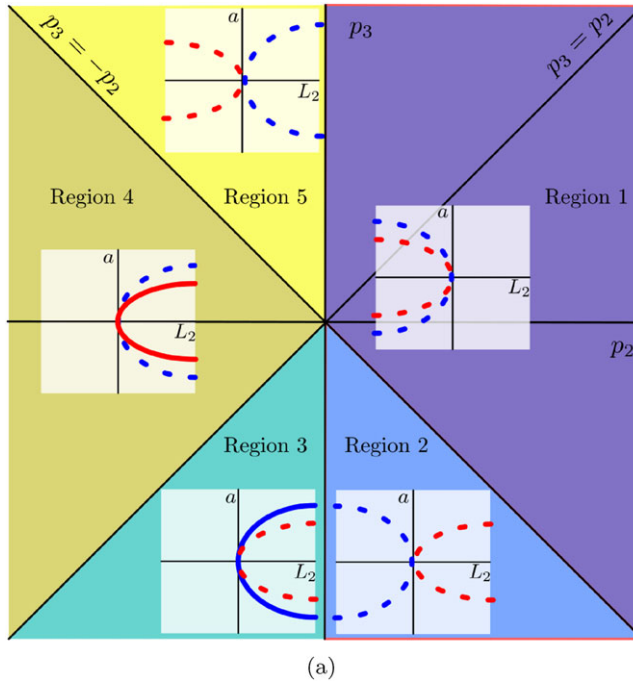


**Figure 8.** Illustrating the bifurcation structures of equations (4.2) and (4.3) in the different parts of the  $(p_2, p_3)$  plane. In each sector, a schematic diagram of the bifurcation branches is shown. The blue and red curves illustrate the  $a_1$  and  $a_2$  amplitudes, respectively and the solid and dashed line styles represent stable and unstable steady states, respectively. Note that the relative amplitudes between the red and blue curves are simply for illustrative purposes.

stability requires  $\lambda_{\bullet 2} < 0$  meaning  $p_2 - p_3 < 0$ . From these last two results concerning  $\lambda_{|2}$  and  $\lambda_{\bullet 2}$ , we recover the known result that spots and stripes cannot both have stable branches stemming from the bifurcation point [63].

We illustrate the possible bifurcation structures in figure 8, where we observe that there are five possible stereotypical structures. Notably, bifurcation structures that give rise to stable trajectories (Regions 3 and 4) make up less than half of the  $(p_2, p_3)$  space.

Although the  $(p_2, p_3)$  graph is the most general way of seeing the possible bifurcation structures of equations (4.2) and (4.3) this does not mean all are possible in a given Turing system. Using the current system of equations (3.17) and (3.18), we illustrate in figure 9a the existence of Regions 1–5 in the  $(D, G_2, G_3)$  space having fixed  $\alpha$ . Figure 9 can be compared with figure 7a where we see that the delineation between the super and subcritical bifurcations of the one-dimensional system matches the volume that would encapsulate Regions 3–5, or  $p_2 < 0$ , which are predicted to lead to supercritical bifurcations for the linear patterns.

Although figure 9a provides us with an understanding of the relative positions of the Regions we are unable to see their structure due to figure 9a not being transparent. Thus, we provide shaded three-dimensional visualizations of the boundary of each section in figure 9b, where we can see that each region has a cone shape in which their cross sections are approximately constant, but they get smaller as  $D$  reduces.

To further aid understanding of the mapping between the  $(D, G_2, G_3)$  and  $(p_2, p_3)$  spaces, we use figure 10a–c to illustrate the influence of mapping horizontal and vertical lines from the  $(D, G_2, G_3)$  space to the  $(p_2, p_3)$  space. Critically, we see that the lines become more warped as  $G_2 \rightarrow 5$  (the boundary of the Turing patterning parameter space). For example, if we consider the horizontal lines of figure 10c only a small part of the horizontal lines lie within Region 1; however, if we consider the mapped lines in figure 10d the curves are distorted such that most

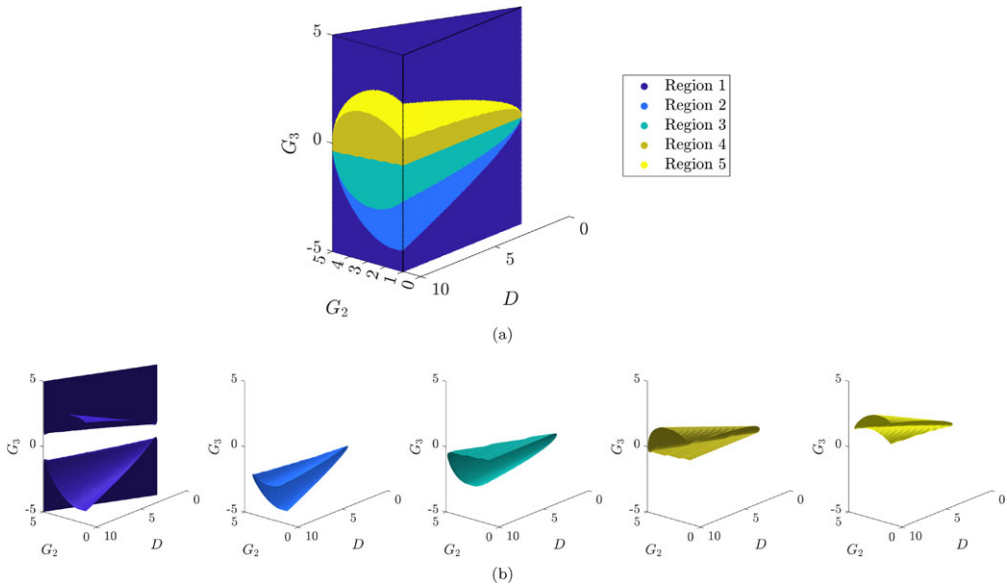


**Figure 9.** Visualizing the mapping between the points of the  $(D, G_2, G_3)$  space and the  $(p_2, p_3)$  space using the relationships from equations (3.19) and (4.4) with  $\alpha = 1$ . Panel (a) shows how all of the regions fit together, while (b) illustrates the bounding surfaces of each region allowing the reader a better understanding of each region's transformed shape. The colour of each region is consistent across all figures referencing them.

of their arclength lies in Region 1, meaning that the values of  $(p_2, p_3)$  become more sensitive to changes in the values of  $(G_2, G_3)$  for  $G_2 \approx 5$ .

To illustrate the success of the maps, we now numerically extract the bifurcation structure across five points, one for each region. The points are chosen along the line  $G_2 = 2$  and can be seen in the  $(G_2, G_3)$  and  $(p_2, p_3)$  planes, figure 10e,f, respectively. Notably, each point is labelled with the corresponding subfigure letter.

Clearly, figure 10g–k matches the derived nonlinear structures in figure 8, even if only within the weakly nonlinear regime close to  $L_c = \sqrt{2}\pi \approx 4.4$ . For example, the parameters for figure 10g,  $(G_2, G_3) = (2, -5)$ , place system (equations (3.17) and (3.18)) in Region 1, meaning that both the line and spot pattern solutions should bifurcate as a subcritical pitchfork and both structures should be unstable. Correspondingly, both the red and blue lines bifurcate into the  $L < L_c$  region and the branches are both unstable. However, the solutions contrast in that the spot solution branch (red line) is never stable and is fully contained within the  $L < L_c$  region, whereas the line solution branch curves back on itself to have a non-trivial stable region for  $4.33 \lesssim L \lesssim 4.65$ . Thus, we see that although the analysis is correct near to  $L_c$ , the strongly nonlinear regime provides stable pattern solutions that are outside our understanding and can only be reliably understood through simulation.

Similarly, we are able to reproduce the weakly nonlinear results from figure 8 in figure 10h. That is, both solutions bifurcate with unstable branches, but the line solutions have a subcritical bifurcation and the spot solutions have a supercritical bifurcation. In the nonlinear regime, the results are once again changed as both branches curve to have stable solutions in the  $L > L_c$  region. Thus, both line and spot patterns are stable for a domain of length  $L \approx 5$ . From the chosen parameters, this is the only simulation to illustrate both solutions being simultaneously stable. This is not to say that the other regions could not also potentially support multiple solutions, but these would require a simulation-driven approach to find.

Figures 10i (parameters from Region 3) and 10j (parameters from Region 4) are perhaps the most useful results as they contain the only branches that bifurcate in a stable manner.

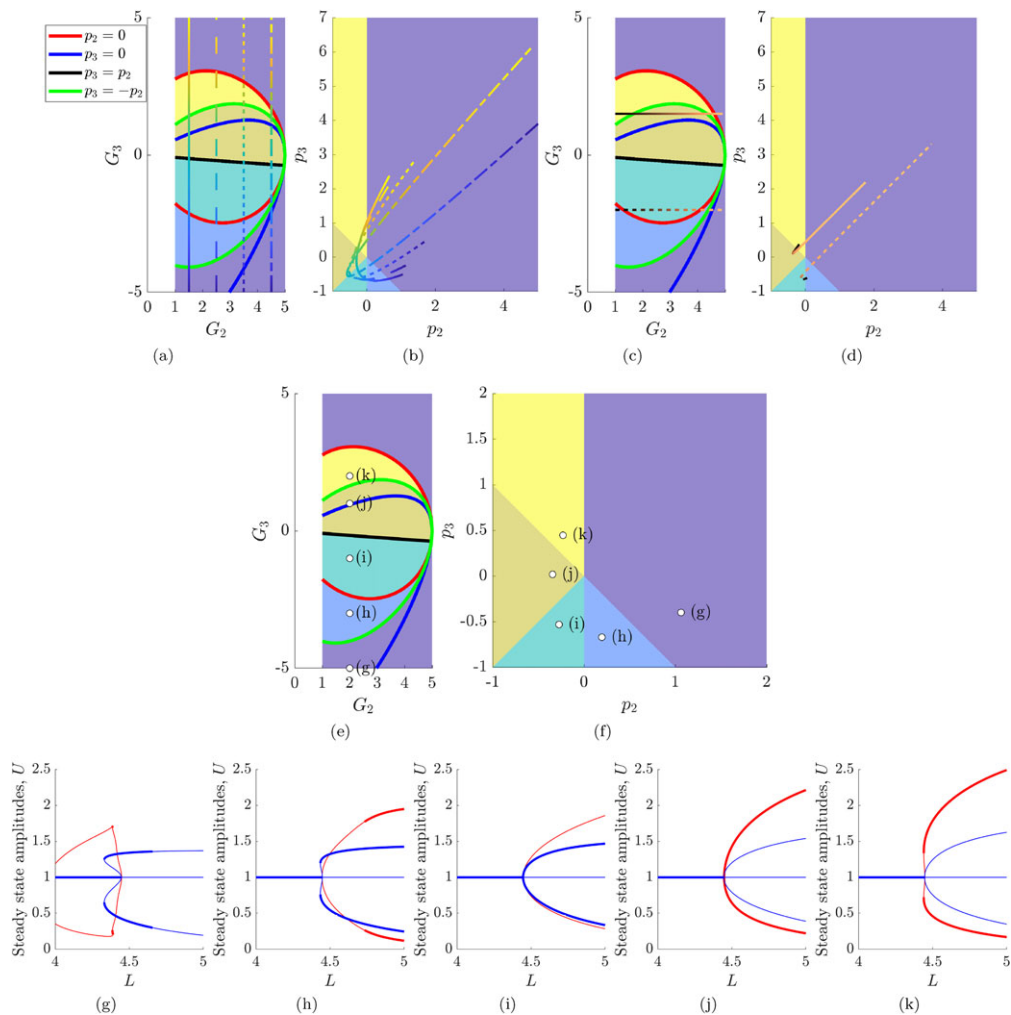


**Figure 10.** Visualizing the mapping of vertical and horizontal lines between  $(G_2, G_3)$  space and the  $(p_2, p_3)$  space using the relationships from equations (3.19) and (4.4) with  $\alpha = 1$  and  $D = 10$ . The colours define the regions as in figures 8 and 9 and bounding lines are defined in the legend of (a). The vertical and horizontal lines in (a) and (c) match those in (b) and (d), respectively. The colour gradient along the lines also match allowing us to visualize how the arclength is distorted between the two spaces. In (e) and (f), we illustrate five points,  $(G_2, G_3) = (2, -5), (2, -3), (2, -1), (2, 1), (2, 2)$ , in the  $(G_2, G_3)$  and  $(p_2, p_3)$  planes, respectively, that are then used in the bifurcation simulations of (g)–(k). Each of the points in (e) and (f) are labelled with the accompanying subfigure labels. For (g)–(k), the blue line tracks the linear solution amplitudes,  $a_l$ , and the red line tracks the spot solution amplitude,  $a_s$ . The thick and thin lines represent the stable and unstable solutions, respectively.

Thus, at least close to  $L_c$ , we can guarantee which pattern will appear. All branches bifurcate supercritically, but only the line solution is stable in Region 3 (figure 10i) and only the spot solution is stable in Region 4 (figure 10j). This is in contrast to all other regions (figure 10g,h and k) where although stable branches might exist they are not contained within the weakly nonlinear expansion region and, thus, we would need simulation to find the solutions and their stability.

Considering the shape and boundaries of the different solutions in figures 9 and 10 we can see that the easiest way to change between the bifurcation structures is to vary  $G_3$  from negative to positive allowing the crossing of all regions (figure 10a,b). Moreover, due to the non-monotonic nature of the boundaries of the regions, varying  $G_2$  can also lead to changing bifurcation structure, but in a nonlinear way.

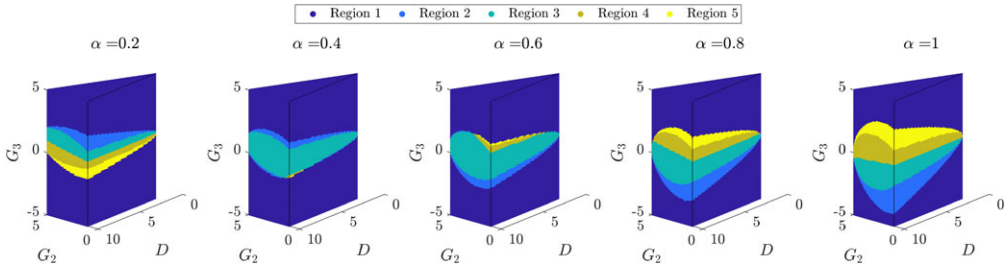


**Figure 11.** Visualizing the influence of varying the steady-state parameter,  $\alpha$  (noted above each subplot), on the  $(D, G_2, G_3)$  space using the relationships from equations (3.19) and (4.4). The colour of each region matches is given in the legend.

For example, suppose we chose a set of  $(G_2, G_3)$  parameter values in Region 3 near the minimum point of the red curve ( $p_2 = 0$ ) in figure 10c. Increasing, or decreasing  $G_2$  would cause the parameters to move into Region 2. Similarly, if we were to choose  $(G_2, G_3)$  parameter values near the maximum of the green curve in Region 4 then increasing or decreasing  $G_2$  would lead to a transition into Region 5 (figure 10c,d).

However, as discussed, it is the transitions between Regions 3 and 4 that are perhaps the most useful to understand because it is only these pattern transitions that we can accurately predict. Critically, it is the ability to transition between spots and stripes that is often used to justify a particular set of kinetics.

Unfortunately, the boundary between Regions 3 and 4 (black line,  $p_3 = p_2$ ) is monotonic, thus, changing only one parameter can only ever lead to one form of bifurcation transition. For example, a line-to-spot transition occurs from Regions 3 to 4 through increasing  $G_2$ , or  $G_3$ . However, if we have the freedom to alter both then we can transition between the regions in either direction through judicious increases and decreases of the variables.

For example, if we start in Region 4 and increase  $G_2$  and simultaneously decrease  $G_3$  it is possible to transition into Region 3. Alternatively, if we start in Region 3 and increase  $G_2$  while increasing  $G_3$  simultaneously we will transition for Region 3 to 4. Thus, a stripe-to-spot transition, or a spot-to-stripe transition can both be observed under an increase in  $G_2$ , as long as we have freedom in  $G_3$ .

The same can be seen to be true if we were to decrease  $G_2$  instead. Once again, we use the freedom in  $G_3$  to drive the desired pattern transition, whether it is spot-to-stripe, or stripe to spot. Hence, we can transition between Regions 3 and 4 in any direction we like, with increasing, or decreasing  $G_2$ .

We can achieve the same results if we were to swap the variables. However, the results would be more sensitive to changes in  $G_3$ , as there are certain values of  $G_3$  that restrict which regions we can enter regardless of whether we increase or decrease  $G_2$  (figure 9a).

Finally, we consider the influence of  $\alpha$  on the bifurcation structure. Intuitively, since  $\alpha$  primarily controls the steady states we might not expect  $\alpha$  to change much of the structure of the regions from figure 9a, which are defined by the nonlinear aspects of the kinetics. However, as we see in figure 11, changes in  $\alpha$  can completely flip the structure of the regions. Whereas previously we have been using  $\alpha = 1$  and Regions 1–5 lie on top of one another, with the region number increasing as  $G_3$  increases, the opposite is true when for  $\alpha = 0.2$ , where the region number increases as  $G_3$  decreases. From simulations beyond  $\alpha = 1$  the structure of the regions stay the same as in the case of  $\alpha = 1$ , the regions just get larger.

Considering Regions 3 and 4 as being the most useful, we observe that as  $\alpha$  increases from 0.2 to 0.8 Region 3 increases in size and Region 4 shrinks from below Region 3 to appear above Region 3. Hence, we see that if there is any flexibility in any two of the parameters of  $D$ ,  $\alpha$ ,  $G_2$  or  $G_3$  we could build relationships that would allow us to move between Regions 3 and 4 in any desired manner.

## 5. Conclusion

We have created a Turing patterning reaction–diffusion system that has an infinite patterning parameter space and is guaranteed to generate positive solutions, assuming positive initial conditions. Moreover, we have demonstrated that the patterning parameter space and final pattern form can be fully defined by just four parameters: the movement rate,  $D$ ; the steady state,  $\alpha$ ; the linear dynamics,  $G_2$ ; the nonlinear dynamics,  $G_3$ . Furthermore, when there is freedom in any two of these parameters, families of relationships between them enable the generation of any desired two-dimensional pattern transition, whether from spots-to-stripes or stripes-to-spots. Identifying such transitions in the data and comparing them to model outcomes has long been a post hoc justification for kinetic choice.

Our findings highlight that qualitative pattern features and transitions alone do not sufficiently constrain reaction–diffusion systems. This flexibility, while a strength in suggesting Turing patterns are more plausible, or likely, than previously thought, undermines their interpretability and emphasizes the need for stronger links to biological pathways and mechanisms.

The variability in biological data used to constrain the model must also be considered. For instance, steady-state protein values are often assumed to be known in experiments. However, as shown in figure 11, small changes in  $\alpha$  (representing the ratio of steady states) can completely alter the bifurcation transition structures. Thus, even minor variability in this ratio could mean the difference between kinetic changes resulting in a spot-to-stripe transition versus a stripe-to-spot transition.

A primary limitation of this work is that the results are confined to the weakly nonlinear regime and are valid only for the first bifurcation. While this approach is useful for identifying promising parameter spaces and demonstrating the feasibility of particular results, understanding solution patterns in the strongly nonlinear regime, where multiple wave modes interact and form superpositions, remains a significant challenge. Exploring Turing systems in such nonlinear regimes is currently better served by rapid simulations and parameter sweeps, rather than ad hoc theory.

Note, we are not advocating for a wholesale shift towards models that prioritize biological realism at the expense of generality. Phenomenological models serve as valuable testing grounds, enabling rapid hypothesis generation, assessing the consistency of current knowledge and offering broad theories of biological understanding. For example, figure 7a illustrates that the subcritical pitchfork bifurcation parameter space is larger than the supercritical bifurcation parameter space. Thus, theoretically, subcritical pitchforks could be more generic than supercritical ones. This is potentially a biologically applicable insight since subcritical bifurcations expand the regions in which patterning can occur, enhancing the plausibility of Turing patterns in biological systems by demonstrating that they occupy larger parameter spaces than previously thought [45].

However, the ability to rapidly generate hypotheses using model components that lack full justification introduces the risk of developing alternative, equally plausible models that yield contradictory predictions. Proving the impossibility of such alternative results is exceedingly difficult, given the infinite number of potential models.

John von Neumann's famous quip, 'With four parameters I can fit an elephant, and with five I can make him wiggle his trunk' [64], highlights how easily complex models can produce complex results. In this work, we have shown that while we may not be able to fit an elephant with four parameters, we can certainly fit zebras, leopards and all transitions between them. This flexibility highlights a critical responsibility of applied mathematicians: as models grow more complex (especially with the advent of machine learning algorithms using hundreds of free parameters [65,66]) it becomes essential to rigorously validate if all model complexity is required. Testing frameworks to their theoretical and practical limits ensures that each assumption and parameter is justified and necessary for capturing observations.

Turing's theory exemplifies this perfectly, its emergent pattern formation arises from the coupling of simpler components that do not pattern. This demonstrates the importance of

disciplined model evaluation, even in the face of growing computational power and modelling capabilities.

Beyond investigating the theoretical systems, we also encourage better use of experimental data. Many mathematical modelling approaches are parametrized based on steady-state information, implicitly assuming that the biological system has stopped evolving, which is an assumption that troubled Turing [3]. However, techniques are beginning to appear that make use of previously ignored transient dynamic data, which further constrain possible Turing systems [67].

Mathematical biologists often rely on prototype dynamics or toy models, combining them to generate greater complexity based on a general understanding of their interactions [5,68]. This approach reflects biology's use of conserved pathways to regulate diverse phenomena [69]. Although revisiting established concepts and applying them to new contexts is a powerful strength, we must remain cautious about introducing unnecessary complexity. Simpler systems may often suffice, matching the tendency of evolution to conserve and repurpose existing components for multiple functions [70,71]. By challenging ourselves to simplify our models, we move closer to understanding the true complexity of biological systems.

**Data accessibility.** All numerical codes and plotted data can be found at [72]. Maple workbooks, MATLAB code and all numerical codes and plotted data can be found at [73].

**Declaration of AI use.** I have not used AI-assisted technologies in creating this article.

**Authors' contributions.** T.W.: conceptualization, data curation, formal analysis, investigation, methodology, project administration, validation, visualization, writing—original draft, writing—review and editing.

**Conflict of interest declaration.** I declare I have no competing interests.

**Funding.** I received no funding for this study.

## Appendix A. Amplitude equation parameter signs

### (a) $p_1$ is guaranteed to be positive in the Turing patterning region

In §3, we concluded that parameter  $p_1$  of equation (3.13) must be positive to ensure that the Turing patterns bifurcate from a stable homogeneous state. Explicitly,

$$p_1 = \frac{2L_2\pi^2(D(L_c^2 - \pi^2)^2 - G_1L_c^4)}{L_c^3((L_c^2 - \pi^2)^2 - G_1L_c^4)}. \quad (\text{A } 1)$$

To show that  $p_1 > 0$  within the parameter region defined by equations (2.27) and (2.28) we are going to show that the numerator and denominator of  $p_1$  are both negative. Firstly, we note

$$2Dk_{\pm}^2 = D - G_2 \pm \sqrt{(D - G_2)^2 - 4D(G_1 - G_2)}, \quad (\text{A } 2)$$

$$\implies 2Dk_{\pm}^2 < 2(D - G_2) \quad \text{since } G_1 > G_2, \quad (\text{A } 3)$$

$$\implies k_{\pm}^2 < 1 - \frac{G_2}{D} < 1. \quad (\text{A } 4)$$

Hence  $L_c = \pi/k_+ > \pi$ . Moreover,

$$\left(1 - \frac{\pi^2}{L_c^2}\right)^2 < 1 \quad \text{for } L_c > \pi. \quad (\text{A } 5)$$

Since, in the Turing parameter region,

$$G_1 > 1 > \left(1 - \frac{\pi^2}{L_c^2}\right)^2, \quad (\text{A } 6)$$

then we deduce that the denominator of equation (A 1) is negative.

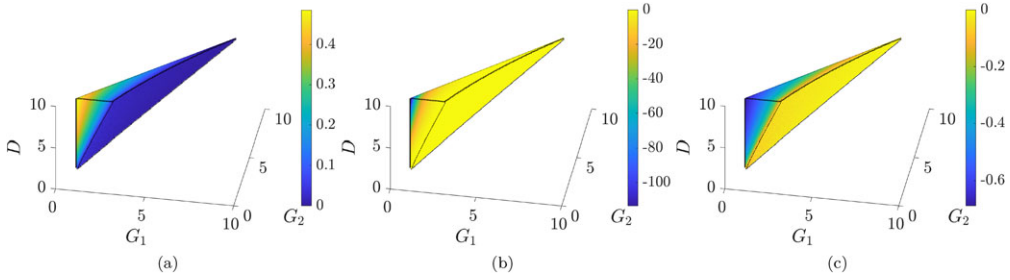


**Figure 12.** Plots of (a)  $p_1$  from equation (A 1), (b) the discriminant from equation (A 10) and (c)  $p_{20}$  from equation (A 9) evaluated over  $200^3$  points forming a regular cubic lattice over the region  $[0, 10] \times [0, 10] \times [0, 10]$ . Only the points within the Turing patterning parameter region are visualized. The colour bars represent the values of each parameter at each point in the space and demonstrates that the parameters do not change sign.

The sign of the numerator is governed by the sign of  $(D(L_c^2 - \pi^2)^2 - G_1 L_c^4)$ . Substituting in  $L_c$  from equation (2.29) and manipulating the variables we find that

$$\begin{aligned} & D(L_c^2 - \pi^2)^2 - G_1 L_c^4 \\ &= \frac{\left( (-D^2 + (3G_1 - G_2)D - G_1 G_2) \sqrt{D^2 + (2G_2 - 4G_1)D + G_2^2} + (D - G_1)(D^2 + (2G_2 - 4G_1)D + G_2^2) \right) \pi^6 L_2}{(G_1 - G_2)^2}, \\ &= A \sqrt{D^2 + (2G_2 - 4G_1)D + G_2^2} + B, \end{aligned}$$

for some  $A$  and  $B$ . Thus, if the numerator is ever zero then

$$A^2(D^2 + (2G_2 - 4G_1)D + G_2^2) - B^2 = 0. \quad (\text{A } 7)$$

However,

$$A^2(D^2 + (2G_2 - 4G_1)D + G_2^2) - B^2 = 4(G_1 - G_2)^2 G_1 (D^2 + (2G_2 - 4G_1)D + G_2^2) D > 0, \quad (\text{A } 8)$$

for parameters in the patterning parameter region. Thus, the numerator of  $p_1$  is never zero and, thus, can never change sign. By evaluating the numerator at a suitable point, e.g.  $(D, G_1, G_2) = (10, 3, 2)$ , we find that the numerator must always be negative, hence,  $p_1 > 0$  for all parameters in the patterning parameter region. This is confirmed in figure 12a.

### (b) $p_2$ does not change sign without additional nonlinearities

Demonstrating that  $p_2$  of equation (3.13) does not change sign within the Turing patterning region of equations (2.25) and (2.26) is less simple than working with  $p_1$  and we must turn to some numerical evaluation to support our conclusion. The explicit form of  $p_2$  is extremely cumbersome to work with and is a function of  $(\alpha, G_1, G_2, D)$ , making it difficult to visualize [18]. However, we note that we can rewrite  $p_2$  as

$$p_2 = p_{22}\alpha^2 + p_{21}\alpha + p_{20}, \quad (\text{A } 9)$$

where the  $p_{2i}$  terms are functions of  $(G_1, G_2, D)$  only. If  $p_2$  were to change sign within the Turing region, there must be a points at which  $p_2 = 0$ . For this to occur for real  $\alpha$  the discriminant of  $p_2$  (as a quadratic in  $\alpha$ ),

$$\Delta = p_{21}^2 - p_{22}p_{20}, \quad (\text{A } 10)$$

must be positive. Being only a function of  $(G_1, G_2, D)$  we can evaluate the discriminant over the Turing patterning region (figure 12b), where we find that the discriminant is non-singular and always negative. Thus  $p_2$  cannot change sign. Since  $p_{20} < 0$  (figure 12c),  $p_2$  must be always

negative in the patterning parameter region. Hence, equations (2.25) and (2.26) must always produce a supercritical Turing bifurcation.

## References

1. Woolley TE. 2014 *50 visions of mathematics*, ch. 48. Mighty Morphogenesis. Oxford, UK: Oxford University Press.
2. Maini PK, Woolley TE, Baker RE, Gaffney EA, Lee SS. 2012 Turing's model for biological pattern formation and the robustness problem. *Interface Focus* **2**, 487–496. (doi:10.1098/rsfs.2011.0113)
3. Turing AM. 1952 The chemical basis of morphogenesis. *Phil. Trans. R. Soc. Lond. B* **237**, 37–72. (doi:10.1098/rstb.1952.0012)
4. Maini PK, Woolley TE. 2019 *The Turing model for biological pattern formation*, pp. 189–204. Berlin, Germany: Springer.
5. Murray JD. 2003 *Mathematical biology II: spatial models and biomedical applications*, vol. 2, 3rd edn. Berlin, Germany: Springer.
6. Kondo S, Miura T. 2010 Reaction-diffusion model as a framework for understanding biological pattern formation. *Science* **329**, 1616–1620. (doi:10.1126/science.1179047)
7. Warne DJ, Baker RE, Simpson MJ. 2019 Using experimental data and information criteria to guide model selection for reaction–diffusion problems in mathematical biology. *Bull. Math. Biol.* **81**, 1760–1804. (doi:10.1007/s11538-019-00589-x)
8. Clermont G, Zenker S. 2015 The inverse problem in mathematical biology. *Math. biosci.* **260**, 11–15. (doi:10.1016/j.mbs.2014.09.001)
9. Maclaren OJ, Nicholson R. 2019 What can be estimated? Identifiability, estimability, causal inference and ill-posed inverse problems. (<http://arxiv.org/abs/1904.02826>).
10. Economou AD, Ohazama A, Porntaveetus T, Sharpe PT, Kondo S, Basson MA, Gritli-Linde A, Cobourne MT, Green JBA. 2012 Periodic stripe formation by a Turing mechanism operating at growth zones in the mammalian palate. *Nat. Genet.* **44**, 1546–1718. (doi:10.1038/ng.1090)
11. Kondo S, Asai R. 1996 Turing patterns in fish skin? *Nature* **380**, 678–678. (doi:10.1038/380678b0)
12. Sheth R, Marcon L, Bastida MF, Junco M, Quintana L, Dahn R, Kmita M, Sharpe J, Ros MA. 2012 Hox genes regulate digit patterning by controlling the wavelength of a Turing-type mechanism. *Science* **338**, 1476–1480. (doi:10.1126/science.1226804)
13. Woolley TE, Baker RE, Tickle C, Maini PK, Towers M. 2014 Mathematical modelling of digit specification by a sonic hedgehog gradient. *Dev. Dynam.* **243**, 290–298. (doi:10.1002/dvdy.24068)
14. Cho SW *et al.* 2011 Interactions between shh, sostdc1 and wnt signaling and a new feedback loop for spatial patterning of the teeth. *Development* **138**, 1807–1816. (doi:10.1242/dev.056051)
15. Glover JD *et al.* 2023 The developmental basis of fingerprint pattern formation and variation. *Cell* **186**, 940–e20956. (doi:10.1016/j.cell.2023.01.015)
16. Barrio RA, Baker RE, Vaughan Jr B, Tribuzy K, de Carvalho MR, Bassanezi R, Maini PK. 2009 Modeling the skin pattern of fishes. *Phys. Rev. E* **79**, 31908. (doi:10.1103/PhysRevE.79.031908)
17. Woolley TE, Krause AL, Gaffney EA. 2021 Bespoke Turing systems. *Bull. Math. Biol.* **83**, 1–32. (doi:10.1007/s11538-021-00870-y)
18. Woolley TE. 2022 Boundary conditions cause different generic bifurcation structures in Turing systems. *Bull. Math. Biol.* **84**, 1–38. (doi:10.1007/s11538-022-01055-x)
19. Woolley TE. 2025 Pattern formation on regular polygons and circles. *J. Nonlinear Sci.* **35**, 1–44. (doi:10.1007/s00332-024-10096-6)
20. Barrio RA, Varea C, Aragón JL, Maini PK. 1999 A two-dimensional numerical study of spatial pattern formation in interacting Turing systems. *Bull. Math. Biol.* **61**, 483–505. (doi:10.1006/bulm.1998.0093)
21. Leppänen T. 2004 *Computational studies of pattern formation in Turing systems*. PhD thesis.
22. Varea C, Hernández D, Barrio RA. 2007 Soliton behaviour in a bistable reaction diffusion model. *J. Math. Biol.* **54**, 797–813. (doi:10.1007/s00285-007-0071-0)
23. Woolley TE, Baker RE, Maini PK, Aragón JL, Barrio RA. 2010 Analysis of stationary droplets in a generic Turing reaction-diffusion system. *Phys. Rev. E* **82**, 051929. (doi:10.1103/PhysRevE.82.051929)

24. Barrio RA. 2008 Physics of emergence and organization. In *chapter Turing systems: a general model for complex patterns in nature* (ed. Ignazio Licata), pp. 267–296. Singapore: World Scientific.
25. Maini PK, Woolley TE, Gaffney EA, Baker RE. 2016 The once and future Turing. In *Biological pattern formation* (eds S. Barry Cooper, Andrew Hodges), ch. 15. Cambridge, UK: Cambridge University Press.
26. Diego X, Marcon L, Müller P, Sharpe J. 2018 Key features of Turing systems are determined purely by network topology. *Phys. Rev. X* **8**, 021071. (doi:10.1103/PhysRevX.8.021071)
27. Marcon L, Diego X, Sharpe J, Müller P. 2016 High-throughput mathematical analysis identifies Turing networks for patterning with equally diffusing signals. *eLife* **5**, e14022. (doi:10.7554/eLife.14022)
28. Klika V, Baker RE, Headon D, Gaffney EA. 2012 The influence of receptor-mediated interactions on reaction-diffusion mechanisms of cellular self-organisation. *Bull. Math. Biol.* **74**, 935–957. (doi:10.1007/s11538-011-9699-4)
29. McCartin BJ. 2008 On polygonal domains with trigonometric eigenfunctions of the Laplacian under Dirichlet or Neumann boundary conditions. *Appl. Math. Sci.* **2**, 2891–2901.
30. Krause AL, Klika V, Woolley TE, Gaffney EA. 2018 Heterogeneity induces spatiotemporal oscillations in reaction-diffusion systems. *Phys. Rev. E* **97**, 052206. (doi:10.1103/PhysRevE.97.052206)
31. Krause AL, Klika V, Woolley TE, Gaffney EA. 2020 From one pattern into another: analysis of Turing patterns in heterogeneous domains via WKBJ. *J. R. Soc. Interface* **17**, 20190621. (doi:10.1098/rsif.2019.0621)
32. Evans LC. 2010 *Partial differential equations*. Graduate studies in mathematics. Providence, RI: American Mathematical Society.
33. Kreyszig E. 2007 *Advanced engineering mathematics*, 8th edn. New York: Wiley-India.
34. Schnakenberg J. 1979 Simple chemical reaction systems with limit cycle behaviour. *J. Theor. Biol.* **81**, 389–400. (doi:10.1016/0022-5193(79)90042-0)
35. Ho WKW *et al.* 2019 Feather arrays are patterned by interacting signalling and cell density waves. *PLoS Biol.* **17**, 1–38. (doi:10.1371/journal.pbio.3000132)
36. Banerjee M. 2015 Turing and non-Turing patterns in two-dimensional prey-predator models. In *Applications of chaos and nonlinear dynamics in science and engineering* (eds Santo Banerjee, Lamberto Rondoni), vol. 4, pp. 257–280. Berlin, Germany: Springer.
37. Woolley TE, Baker RE, Maini PK. 2017 The Turing guide. In *Turing's theory of morphogenesis*, (eds Jack Copeland, Jonathan Bowen, Mark Sprevak, Robin Wilson) ch. 35. Oxford, UK: Oxford University Press.
38. Krause AL, Gaffney EA, Jewell TJ, Klika V, Walker BJ. 2024 Turing instabilities are not enough to ensure pattern formation. *Bull. Math. Biol.* **86**, 21. (doi:10.1007/s11538-023-01250-4)
39. Ni W, Tang M. 2005 Turing patterns in the Lengyel-Epstein system for the CIMA reaction. *T. Am. Math. Soc.* **357**, 3953. (doi:10.1090/S0002-9947-05-04010-9)
40. Rudovics B, Dulos E, De Kepper P. 1996 Standard and nonstandard Turing patterns and waves in the CIMA reaction. *Phys. Scr.* **T67**, 43–50. (doi:10.1088/0031-8949/1996/T67/009)
41. De Kepper P, Castets V, Dulos E, Boissonade J. 1991 Turing-type chemical patterns in the Chlorite-Iodide-Malonic Acid reaction. *Physica D* **49**, 161–169. (doi:10.1016/0167-2789(91)90204-M)
42. Woolley TE, Baker RE, Maini PK. 2017 Turing's theory of morphogenesis: where we started, where we are and where we want to go. In *The incomputable: journeys beyond the Turing barrier* (eds S. Barry Cooper, Mariya I. Soskova), pp. 219–235.
43. Ward MJ, McInerney D, Houston P, Gavaghan D, Maini P. 2002 The dynamics and pinning of a spike for a reaction-diffusion system. *SIAM J. Appl. Math.* **62**, 1297–1328. (doi:10.1137/S0036139900375112)
44. Ward MJ, Wei J. 2002 The existence and stability of asymmetric spike patterns for the Schnakenberg model. *Stud. App. Math.* **109**, 229–264. (doi:10.1111/1467-9590.00223)
45. Murray JD. 1982 Parameter space for Turing instability in reaction diffusion mechanisms: a comparison of models. *J. Theor. Biol.* **98**, 143. (doi:10.1016/0022-5193(82)90063-7)
46. Korvasová K, Gaffney EA, Maini PK, Ferreira MA, Klika V. 2015 Investigating the Turing conditions for diffusion-driven instability in the presence of a binding immobile substrate. *J. Theor. Biol.* **367**, 286–295. (doi:10.1016/j.jtbi.2014.11.024)

47. Bozzini B, Gambino G, Lacitignola D, Lupo S, Sammartino M, Sgura I. 2015 Weakly nonlinear analysis of Turing patterns in a morphochemical model for metal growth. *Comput. Math. Appl.* **70**, 1948–1969. (doi:10.1016/j.camwa.2015.08.019)
48. Grindrod P. 1996 *The theory and applications of reaction-diffusion equations: patterns and waves*. Oxford applied mathematics and computing science series. Oxford, UK: Clarendon Press.
49. Auchmuty JFG, Nicolis G. 1975 Bifurcation analysis of nonlinear reaction-diffusion equations—I. Evolution equations and the steady state solutions. *Bull. Math. Biol.* **37**, 323–365. (doi:10.1016/S0092-8240(75)80036-X)
50. Wollkind DJ, Manoranjan VS, Zhang L. 1994 Weakly nonlinear stability analyses of prototype reaction-diffusion model equations. *SIAM Rev.* **36**, 176–214. (doi:10.1137/1036052)
51. Nicolis G. 1995 *Introduction to nonlinear science*. Cambridge, UK: Cambridge University Press.
52. Kevorkian JK, Cole JD. 2012 *Multiple scale and singular perturbation methods*. Applied Mathematical Sciences. New York, NY: Springer.
53. Becherer P, Morozov AN, van Saarloos W. 2009 Probing a subcritical instability with an amplitude expansion: an exploration of how far one can get. *Physica D* **238**, 1827–1840. (doi:10.1016/j.physd.2009.03.009)
54. Ramm AG. 2001 A simple proof of the Fredholm alternative and a characterization of the Fredholm operators. *Am. Math. Mon.* **108**, 855–860. (doi:10.1080/00029890.2001.11919820)
55. Maplesoft, a division of Waterloo Maple Inc.: Maple. See <https://hadoop.apache.org>.
56. The MathWorks Inc. MATLAB version: 9.14.0 (r2023a), 2023. See [www.mathworks.com](http://www.mathworks.com).
57. Dutt AK. 2010 Turing pattern amplitude equation for a model glycolytic reaction-diffusion system. *J. Math. Chem.* **48**, 1–15. (doi:10.1007/s10910-010-9699-x)
58. Dutt AK. 2012 Amplitude equation for a diffusion-reaction system: the reversible Sel'kov model. *AIP Adv.* **2**, 042125. (doi:10.1063/1.4765650)
59. Uecker H, Wetzel D, Rademacher JDM. 2014 pde2path – A Matlab Package for Continuation and Bifurcation in 2D Elliptic Systems. *Numer. Math.: Theory, Meth. Appl.* **7**, 58–106. (doi:10.4208/nmtma.2014.1231nm)
60. Dohnal T, Rademacher JDM, Uecker H, Wetzel D. 2014 pde2path 2.0: multi-parameter continuation and periodic domains. In *Proc. of 8th European Nonlinear Dynamics Conf.* (eds H Ecker, A Steindl, S Jakubek), July 6–11, 2014, Vienna, Austria. Vienna, Austria: Vienna University of Technology.
61. Uecker H. 2021 Continuation and bifurcation in nonlinear pdes—algorithms, applications, and experiments. *Jahresber. der Dtsch. Math.-Vereinigung* **124**, 1–38. (doi:10.1365/s13291-021-00241-5)
62. Uecker H. 2021 *Numerical continuation and bifurcation in Nonlinear PDEs*. Philadelphia, PA: SIAM.
63. Ermentrout B. 1991 Stripes or spots? Nonlinear effects in bifurcation of reaction-diffusion equations on the square. *Proc. R. Soc. Lond. A* **434**, 413–417. (doi:10.1098/rspa.1991.0100)
64. Dyson F. 2004 A meeting with enrico fermi. *Nature* **427**, 297–297. (doi:10.1038/427297a)
65. Schnörr D, Schnörr C. 2023 Learning system parameters from Turing patterns. *Mach. Learn.* **112**, 3151–3190. (doi:10.1007/s10994-023-06334-9)
66. Matas-Gil A, Endres RG. 2024 Unraveling biochemical spatial patterns: machine learning approaches to the inverse problem of stationary Turing patterns. *iScience* **27**, 109822. (doi:10.1016/j.isci.2024.109822)
67. Klika V, Gaffney EA, Maini PK. 2024 On the speed of propagation in Turing patterns for reaction-diffusion systems. *Physica D* **467**, 134268. (doi:10.1016/j.physd.2024.134268)
68. Murray JD. 2003 *Mathematical biology I: an introduction*, vol. 1, 3rd edn. Berlin, Germany: Springer.
69. Jacob F. 1977 Evolution and tinkering. *Science* **196**, 1161–1166. (doi:10.1126/science.860134)
70. Conant GC, Wolfe KH. 2008 Turning a hobby into a job: how duplicated genes find new functions. *Nat. Rev. Genet.* **9**, 938–950. (doi:10.1038/nrg2482)
71. Wagner A. 2005 *Robustness and evolvability in living systems*. Princeton, NJ: Princeton University Press.
72. Woolley TE. 2025 Bespoke Turing patterns with specific nonlinear properties. Github. [https://github.com/ThomasEWoolley/Nonlinear\\_properties](https://github.com/ThomasEWoolley/Nonlinear_properties)
73. Woolley TE. 2025 Bespoke Turing patterns with specific nonlinear properties. Zenodo. (doi:10.5281/zenodo.15058356)